

# Discovery of Non-Thermal X-Rays from the Shell of RCW 86

Aya BAMBA and Katsuji KOYAMA\*

*Department of Physics, Graduate School of Science, Kyoto University, Sakyo-ku, Kyoto 606-8502*

*E-mail(AB): bamba@cr.scphys.kyoto-u.ac.jp*

and

Hiroshi TOMIDA

*National Space Development Agency of Japan,*

*World Trade Center Bldg, 2-4-1 Hamamatu-cho, Minato-ku, Tokyo, 105-8060*

(Received 2000 June 16; accepted 2000 July 25)

## Abstract

We report the ASCA (Advanced Satellite for Cosmology and Astrophysics) results of RCW 86, a shell-like supernova remnant (SNR). The bright region in the X-ray band traces the radio clumpy shell, although details of the structure are different. The X-ray spectrum from each part of the shell can not be fitted to a thin thermal plasma model, but requires at least three components: a low-temperature plasma of 0.3 keV, a high-temperature plasma of  $\geq$  several keV, and a power-law component with a photon index of  $\sim 3$ . The abundances of O, Ne, Mg and Si are significantly higher than that of Fe, indicating that RCW 86 is a type II SNR. The absorption column of  $\sim 3 \times 10^{21}$  H cm $^{-2}$  indicates the distance to the SNR to be several kpc. The power-law component can be interpreted to be synchrotron radiation of high-energy electrons. Assuming an energy density equipartition between the magnetic field and the electrons, and using the radio and X-ray spectra, we argue that high-energy electrons are accelerated up to 20 TeV. The acceleration efficiency is, however, different from shell to shell.

**Key words:** acceleration of particles — ISM: individual (RCW 86) — supernova remnants — X-rays: ISM

## 1. Introduction

The origin and acceleration of cosmic rays have been a long-standing key problem since the discovery in 1911–1912 (Hess 1911, 1912). The energy spectrum of cosmic rays is presented by a power-law function with a break at  $\sim 10^{15.5}$  eV, called “knee energy”. The presence of the break in the power-law distribution indicates that cosmic rays may have two different origins. A natural explanation is that cosmic rays below the knee energy are originated in our Galaxy, while those above the knee are of extragalactic origin. The most probable origin and acceleration mechanism of the galactic cosmic rays are the first-order Fermi acceleration process by fast-moving shells of supernova remnants (SNRs) (Wentzel 1974). In fact, radio spectra and polarizations in SNR shells are well represented by synchrotron radiations of high-energy electrons with a power-law distribution of an index expected from the Fermi acceleration process. The radio data thus indicate that GeV energy electrons are accelerated in SNR shells.

If electrons are accelerated to a higher energy near the knee, the energy of synchrotron radiation shifts to an

X-ray band. Shell-like SNRs, however, typically display line-dominated thermal X-rays, with the characteristic temperature of about 1 keV, due to either a single or multi-component plasma. Thus, no evidence for synchrotron X-rays has so far been found. Recently, two shell-type SNRs, SN 1006 and G347.3–0.5, have been found to be dominated by power-law X-rays with no emission line (Koyama et al. 1995, 1997; Slane et al. 1999). The power-law X-rays, together with the discoveries of TeV gamma rays (Tanimori et al. 1998; Muraishi et al. 2000), have indicated that the shells of these SNRs are the acceleration sites of extremely high energy electrons of  $10^{13}$  to  $10^{15}$  eV. In such relativistic energy, protons, the main component of cosmic rays, and electrons are essentially the same, except for the charge polarity (Bell 1978). Therefore, these two SNRs are most probable sites of cosmic-ray accelerations near to “the knee energy”.

Some hints for synchrotron X-rays from other shell-like SNRs are found with ASCA (Advanced Satellite for Cosmology and Astrophysics), RXTE (Rossi X-ray Timing Explorer), and CXO (Chandra X-ray Observatory). Even typical thin thermal SNRs, such as Cas A, IC 443, Tycho, Kepler, G156.2+5.7 and RCW 86 exhibit hard energy tails over the thin thermal emissions. Some of the

\* CREST, Japan Science and Technology Corporation (JST), 4-1-8 Honmachi, Kawaguchi, Saitama 332-0012

hard tails are most likely to be non-thermal (Cas A and IC443; Petre et al. 1997), but the others are controversial, either non-thermal or higher energy plasma of about 10 keV. Since high-energy particles from a higher temperature plasma (e.g.  $\geq 10$  keV) are more easily injected into the “Fermi acceleration machine” than those from a lower temperature plasma (e.g.  $\sim 1$  keV) (Bell 1978), it is essentially important to investigate the relation of a high-energy plasma and non-thermal emission.

RCW 86 was identified as the remnant of the historical supernova in AD 185 (Clark, Stephenson 1977). However Chin and Huang (1994), and Schaefer (1995), derived the age of RCW 86 to be  $\sim 8000$  yr with a Sedov solution. Since RCW 86 is located in an OB star association, it is likely to be a type II SNR (Clark, Stephenson 1977). X-rays from RCW 86 were discovered by Naranan et al. (1977). The X-ray spectrum obtained with the Einstein satellite was represented by a two-temperature plasma model (Winkler 1978). The higher energy spectrum (2.0–20 keV) with the Ginga satellite was explained by a single temperature plasma of  $kT \geq 4$  keV (Kaastra et al. 1992). Using the ASCA satellite, Vink et al. (1997) reported that the plasma temperature varies from region to region of the shells, from 0.8 keV to  $> 3$  keV. Petre et al. (1999) found a hard X-ray tail extending to several 10 keV in the RXTE spectrum. They thus argued that the shell of RCW 86 has a non-thermal emission and is one of the candidates for the origin of high-energy cosmic rays. However, non-imaging instrument of RXTE could not clarify which region of the SNR is the hard X-ray emitter. In this paper, we revisit to the ASCA data and examine whether or from which region RCW 86 is emitting non-thermal hard X-rays.

## 2. Observations

RCW 86 was observed with ASCA (Tanaka et al. 1994) on 1993 August 17–18. X-ray photons are collected with four XRTs (X-Ray Telescopes; Serlemitsos et al. 1995) and detected with two SIS (Solid-state Imaging Spectrometers; Burke et al. 1991) cameras and two GIS (Gas Imaging Spectrometers; Ohashi et al. 1996) on the foci of the XRTs. Three mosaic observations have been conducted, because the size of RCW 86 is larger than the field of view of SIS. The SISs were operated in the 4-CCD read-out mode, with the data acquisition of a faint mode in the High bit rate and a bright mode in the Medium and Low bit rates. No significant degradation is found in the SIS data taken about 6 months after the launch; hence, no correction for the Residual Dark Distribution (RDD) is required (T. Dotani et al. 1997, ASCA News 5, 14). The GISs were operated in the normal PH mode. We excluded high-background data and non-X-ray events with the standard method according to the user guide by NASA Goddard Space Flight Center. Then, the available

exposure times are  $\sim 20$  ks,  $\sim 9$  ks, and  $\sim 8$  ks for each observation.

## 3. Analyses and Results

Figure 1 shows the GIS mosaic images around RCW 86 in the energy bands of 0.7–2.0 keV (figure 1a) and 2.0–10.0 keV (figure 1b), in which vignetting and exposure times are corrected. In both the images, we can see two prominent shells at northeast and southwest of the RCW 86 rim. The sizes and shapes of the X-ray shells are similar to those of H $\alpha$  (Smith 1997) and the 847 MHz band (Kesteven, Caswell 1987). With a quick look, we see different structure between the two energy bands, or the spectrum is different from region to region. In the 0.7–2.0 keV band, the southwest shell is appeared to be boomerang shape, while in the 2.0–10.0 keV band, the shell changes to bar-like structure. The northeast shell is brighter in the hard band than in the soft band. We also detected a point-like spot near to the northeast shell in figure 1a with a significance of  $4\sigma$ .

We made the X-ray spectra from each region with the designation given in figure 1a. Since RCW 86 is located near on the galactic plane, contamination from the galactic ridge plasma emission can not be ignored (Koyama et al. 1986). Hence the background spectrum is taken from outside of RCW 86 but near the same galactic latitude as the source region, and is subtracted from the source spectrum. We first made the spectra from the brightest shell, SW shell (combined with SW-1 and SW-2 shells). Although we treated both the GIS and SIS spectra simultaneously to increase statistics, we show, for simplicity, only the SIS spectrum in figure 2a. Prominent emission lines from highly ionized O, Ne, Mg, Si, and Fe atoms in the spectrum imply that a significant fraction of the X-rays is attributable to a thin thermal plasma. Therefore, we applied a thin thermal model in non-equilibrium ionization (Masai 1984), as was already tried by Vink et al. (1997). This model is statistically rejected with  $\chi^2 = 2154/685$ ; even the abundances of O, Ne, Mg, Si, and Fe are allowed to be free parameters. Large residuals are found in the 1–2 keV and above 5 keV bands. We note that the thermal model reported by Vink et al. (1997) is unacceptable for our GIS and SIS simultaneous fitting. In fact, the iron K-shell line and those from lighter elements such as O, Ne, Mg, and Si can hardly coexist in a single temperature plasma. We thus added another higher temperature thin plasma in non-equilibrium ionization. This two-temperature plasma model is still rejected with  $\chi^2 = 1685/682$ . A significant data excess is found at a high-energy continuum above 6.5 keV. The discrepancy of the model and data become larger in higher energy. In fact, this model spectrum can only account 10% of the RXTE flux at  $> 10$  keV reported by Petre et al. (1999).

Accordingly, we are required to add a non-thermal

(power-law) component, and hence applied a model consisting of two thin thermal plasmas: component 1 (dotted line) and 2 (dashed line), respectively, and a power-law component (solid line, see figure 2a). For simplicity, the absorption column is taken to be common among the three components, and the abundances of O, Ne, Mg, Si, and Fe in component 1 and that of Fe in component 2 are allowed to be free parameters, while the others are fixed to be solar values (Allen 1973).  $\chi^2$  is then greatly reduced to be marginally value of 979/682. Therefore we do not try more complicated models, although this 3-component model is still rejected in a statistical point of view. The best-fit parameters are shown in table 1.

The power-law fluxes extrapolated to higher than 10 keV are smoothly connected to the RXTE results, as is shown in the best-fit model function given in figure 2b. Thus, the hard X-rays observed with RXTE can be regarded to be a higher energy part of the power-law component found with the present ASCA analysis of the brightest shell.

For the diffuse spectra from the other regions of this SNR, we applied the same model as the SW shell, allowing only the normalizations of three components and the ionization parameter to be free; otherwise, the limited photon statistics of these faint regions give no essential constraint on the physical parameters. This simplified model approach is found to be reasonable, because the reduced  $\chi^2$  for the fitting of each region is about 1.5–1.8, comparable to that in the SW shell analysis. The best-fit ionization parameters, fluxes, and the flux ratios for each component are given in table 2.

Figure 3 is a projected profile of RCW 86 to the dotted line given in figure 2b. We can clearly see a hard spot near to the NE shell, with a width of about  $3'$ , corresponding to the spatial resolution of GIS. We thus regard the hard spot to be a point source. The spectrum of the hard spot is taken from a circle of  $3'$  radius on the source, and that of the background is an annulus region of  $3'$ – $6'$  radius around the source. The background subtracted spectrum shows no significant line, and can be fitted to a power-law model of a photon index  $= 2.3^{+0.2}_{-0.2}$  and absorption of  $N_{\text{H}} = 2.0^{+0.9}_{-0.8} \times 10^{21} \text{ cm}^{-2}$  with reduced  $\chi^2 = 51/70$  (hereinafter, errors are 90% confidence). The total flux in the 0.7–10.0 keV band is  $3.7 \times 10^{-12} \text{ erg cm}^{-2} \text{ s}^{-1}$ .

## 4. Discussions

We found that the X-ray spectra of RCW 86 have three components; a lower temperature plasma (component 1), higher temperature plasma (component 2), and a power-law emission (non-thermal component). Since the abundances of light elements such as O, Ne, Mg, and Si are higher than that of Fe, RCW 86 is likely due to a type II SN, consistent with that RCW 86 is in an OB star as-

sociation (Clark, Stephenson 1977). The best-fit column density of  $3.2 \times 10^{21} \text{ H cm}^{-2}$  is also consistent with the distance to the OB star association of 2.5 kpc. Here and after, we adopted this value for the distance to RCW 86. The discovery of the hard spot in RCW 86 is also suggestive of the type II concept. We separately discuss these emissions.

### 4.1. Hard Spot

Since the absorption column of the hard spot is similar to that of the SW shell, we infer that the hard spot is located in the SNR. The total luminosity is then estimated to be  $2.7 \times 10^{33} \text{ erg s}^{-1}$ . This luminosity and the power-law spectrum of a photon index ( $\alpha = 2.3$ ) suggest that hard spot could be a Crab-like pulsar, supporting a type II SN origin. We therefore searched for coherent pulsations using the FFT technique; however, we found no hint of pulsation in the time scale of  $7.825 \times 10^{-3} \text{ s}$  to 16381 s. Obviously, further sensitive searches for coherent pulsations are required.

### 4.2. Higher Temperature Plasma

The nature of component 2 is puzzling because the temperature of  $\geq 10 \text{ keV}$  is unusually high for SNRs. The presence of this high temperature plasma mainly rely on the line features around 6.5 keV, because the continuum emissions above a few keV are not sensitive to separate a high temperature plasma and a power-law emission. Thus, to investigate the origin of the line feature is essentially important. Since the observed line energy is about 6.5 keV near to the K-shell transition energy of neutral or low ionization iron atoms, one may argue that the line is fluorescence from cold iron, like in a molecular cloud Sgr B2 (Murakami et al. 2000). This possibility can be rejected because the column density is too small to emit such strong neutral iron lines by the reflection mechanism. Strong iron lines from rather low ionization atoms are also found in other young SNRs, for example, Tycho and Kepler's SNRs (Hwang, Gotthelf 1997). Borkowski and Szymkowiak (1997) suspected that these iron lines in young SNRs are the composite of lines from a hot plasma and fluorescent lines coming from dust grains. If this is the case of RCW 86, the energy of iron line due to a hot plasma can be higher, and thus the ionization parameter becomes larger. Hence, the true temperature of the hot plasma should be lower than 10 keV, probably around several keV, which is not unusually high for a young SNR.

### 4.3. Lower Temperature Plasma

At the distance of 2.5 kpc, the radius of the shell ( $R$ ) is estimated to be 14 pc. Assumption that SW shell covers  $\pi/2 \text{ sr}$  (see figure 1) and that the thickness is  $1/12R$  (expected from Sedov solution), the density and ionization

age of SW shell are estimated from the luminosity and the ionization parameter  $nt$ , to be 0.45 (0.40–0.50)  $\text{cm}^{-3}$  and 3100 (2500–3700) yr, respectively. For NE shell, we assume the covering solid angle to be  $\pi/4$  sr (see figure 1) and estimate the density and ionization age to be 0.06 (0.04–0.08)  $\text{cm}^{-3}$  and 1800 (1000–3900) yr, respectively. These ionization ages are significantly shorter than the Sedov age of 8000 yr (Chin, Huang, 1994; Schaefer, 1995), and favor that RCW 86 is the remnant of AD 185 (Clark, Stephenson 1977). We note that systematical difference between the ionization age and the Sedov age is found in some other type II SNRs by Hughes et al. (1998). They have systematically analyzed shell-like SNRs in the Large Magellanic Cloud and found some of the type II candidates shows the ionization ages shorter than the Sedov ages. They interpret that these type II SNRs exploded within pre-existing low-density cavities in the interstellar medium. The low interior density allows the SN blast wave to propagate rapidly to the cavity wall, where it then encounters denser gas, begins to slow down, and emits copious amounts of X-rays. This scenario reduces the dynamical ages from that inferred with the Sedov model (Sedov ages). RCW 86 may be the same case, because it is likely a type II in an OB star association (Clark, Stephenson 1977). Thus, the real age would be similar to the ionization age of 3100 yr.

#### 4.4. Power-Law Emission

Figure 4 is the wide band spectrum from RCW 86, in which the radio data is refereed from Green (1998). The spectrum can be explained by a power-law model with a break at  $\sim 2 \times 10^2$  eV. This break is produced by synchrotron energy loss, which is larger for higher energy electrons, and hence gives the maximum electron energy. The synchrotron energy loss is proportional to the square of the magnetic field. The magnetic field is calculated using the IRAS result by Greidanus and Strom (1990) to be 80  $\mu\text{G}$  under the assumption of energy equipartition. We then estimate the highest energy of electrons which have been accelerated in the shell of RCW 86 to be  $\sim 20$  TeV. Actually, many SNRs have smaller magnetic field than that on the assumption of energy equipartition. Therefore, the highest energy of electrons may be higher than our estimation.

The flux ratio of the non-thermal to thermal components is different from region to region. The thermal component is dominant in SW-1 shell, while SW-2 shell has both components. In NE shell, the non-thermal component is dominated. Both components are dim in the inner region, supporting that the non-thermal X-rays do not come from a pulsar nebula. These differences would be related to the difference of the shock intensities, the magnetic fields, and/or field line direction relative to that of the shock propagation. To address these issues, we

need much higher spatial resolution instruments in the hard energy band, such as Chandra and Newton observations.

#### *Note added in proof*

After completing this draft, we have become aware of a pre-print by Borkowski et al. (astro-ph/0006149), which gives essentially the same conclusion with different approach of data analysis.

We are grateful to all members of the ASCA team. Our particular thanks are due to K. Yoshita for fruitful comments and suggestion about NEI models.

#### References

- Allen C.W. 1973, *Astrophysical Quantities*, 3ed (Athlone Press, London) p30
- Bell A.R. 1978, *MNRAS* 182, 147
- Borkowski K.J., Szymkowiak A.E. 1997, *ApJ* 477, L49
- Burke B.E., Mountain R.W., Harrison D.C., Bautz M.W., Doty J.P., Ricker G.R., Daniels P.J. 1991, *IEEE Trans. ED-38*, 1069
- Chin Y.N., Huang Y.N. 1994, *Nature* 371, 398
- Clark D.H., Stephenson F.R. 1977, *The Historical Supernova* (Pergamon, Elmsford, N.Y.) p83
- Green D. A. 2000 *A Catalogue of Galactic Supernova Remnants* (2000 August version), (Mullard Radio Astronomy Observatory, Cambridge, UK (available on the World-Wide-Web at "http://www.mrao.cam.ac.uk/surveys/snrs/")
- Greidanus H., Strom R.G. 1990, *A&A* 240, 385
- Hess V.F. 1911, *Phys. Zeits* 12, 998
- Hess V.F. 1912, *Phys. Zeits* 13, 1084
- Hughes J.P., Hayashi I., Koyama K. 1998, *ApJ* 505, 732
- Hwang U., Gotthelf E.V. 1997, *ApJ* 475, 665
- Kaastra J.S., Asaoka I., Koyama K., Yamauchi S. 1992, *A&A* 264, 654
- Kesteven M.J., Caswell J.L. 1987, *A&A* 183, 118
- Koyama K., Kinugasa K., Matsuzaki K., Nishiuchi M., Sugizaki M., Torii K., Yamauchi S., Aschenbach B. 1997, *PASJ* 49, L7
- Koyama K., Makishima K., Tanaka Y., Tsunemi H. 1986, *PASJ* 38, 121
- Koyama K., Petre R., Gotthelf E.V., Hwang U., Matsuura M., Ozaki M., Holt S.S. 1995, *Nature* 378, 255
- Masai K. 1984 *Ap&SS*, 98, 367
- Muraishi H., Tanimori T., Yanagita S., Yoshida T., Moriya M., Kifune T., Dazeley S.A., Edwards P.G. et al. 2000, *A&A* 354, L57
- Murakami H., Koyama K., Sakano M., Tsujimoto M., Maeda Y. 2000, *ApJ* 534, 283
- Naranan S., Shulman S., Yentis D., Fritz G., Friedman H. 1977, *ApJ* 213, 53
- Ohashi T., Ebisawa K., Fukazawa Y., Hiyoshi K., Horii M., Ikebe Y., Ikeda H., Inoue H. et al. 1996, *PASJ* 48, 157
- Petre R., Allen G.E., Hwang U. 1999, *Astron. Nachr.* 320, 199

- Petre R., Keohane J.W., Gotthelf E.V., Hwang U., Allen G.,  
Koyama K., Ozaki M. 1997, presented at IAUS 188
- Schaefer B.E. 1995, AJ 110, 1793
- Serlemitsos P.J., Jalota L., Soong Y., Kunieda H., Tawara Y.,  
Tsusaka Y., Suzuki H., Sakima Y. et al. 1995, PASJ 47,  
105
- Slane P., Gaensler B.M., Dame T.M., Hughes J.P., Plucinsky  
P.P., Green A. 1999, ApJ 525, 357
- Smith R.C. 1997, AJ 114, 2664
- Tanaka Y., Inoue H., Holt S.S. 1994, PASJ 46, L37
- Tanimori T., Hayami Y., Kamei S., Dazeley S.A., Edwards  
P.G., Gunji S., Hara S., Hara T. et al. 1998, ApJ 497, L25
- Vink J., Kaastra J.S., Bleeker J.A.M. 1997, A&A 328, 628
- Wentzel D.G. 1974, ARA&A 12, 71
- Winkler P.F. Jr 1978, ApJ 221, 220

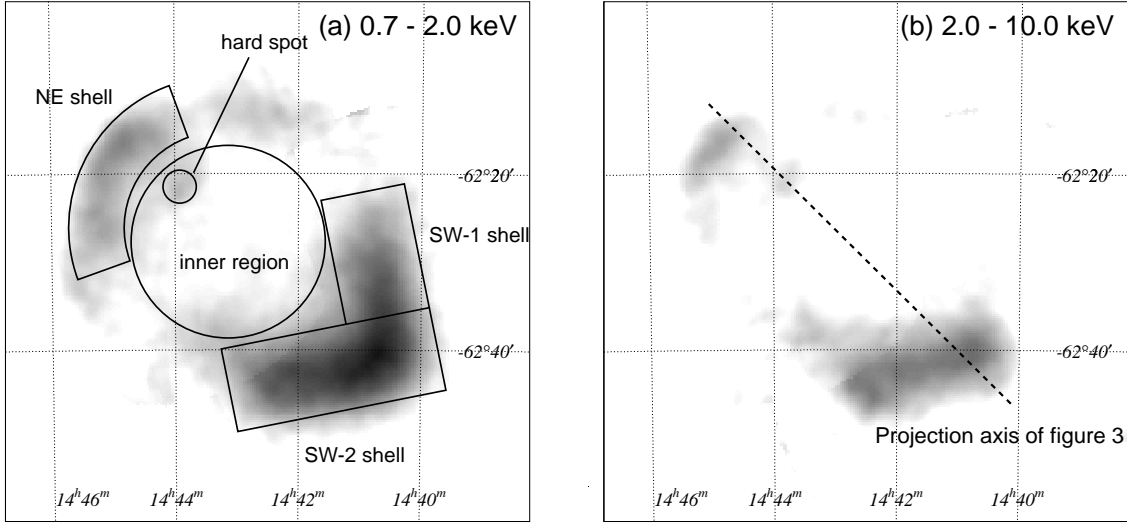


Fig. 1.. Figure 1. Mosaic GIS maps in the 0.7–2.0 keV (a) and the 2.0–10.0 keV (b) bands with J2000 coordinates. Vignetting and exposure time have been corrected. The gray map is drawn in logarithmic scale.

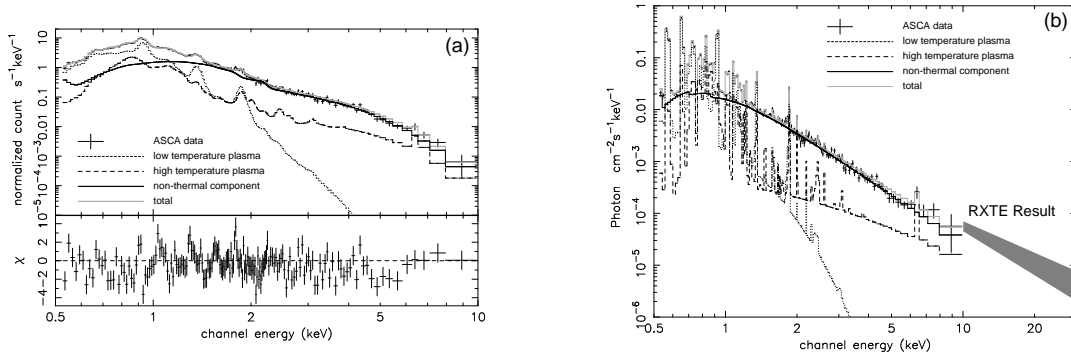


Fig. 2.. (a) The ASCA SIS 0+1 spectra from SW shell of RCW 86 with the best-fit models (upper panel). Residuals from the best-fit models are shown in the lower panel. The dotted, dashed, and solid line represents the best-fit models (see text). (b) The photon flux of the best-fit model. The hatched area represents the photon fluxes and errors with the RXTE observations.

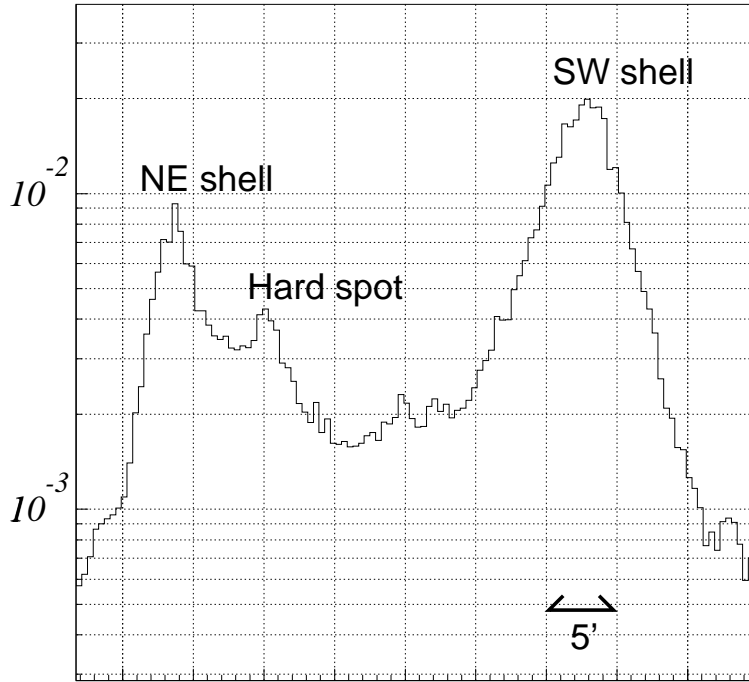


Fig. 3.. The projected profile to the axis given in figure 2b. The vertical axis represents count rate per bin.

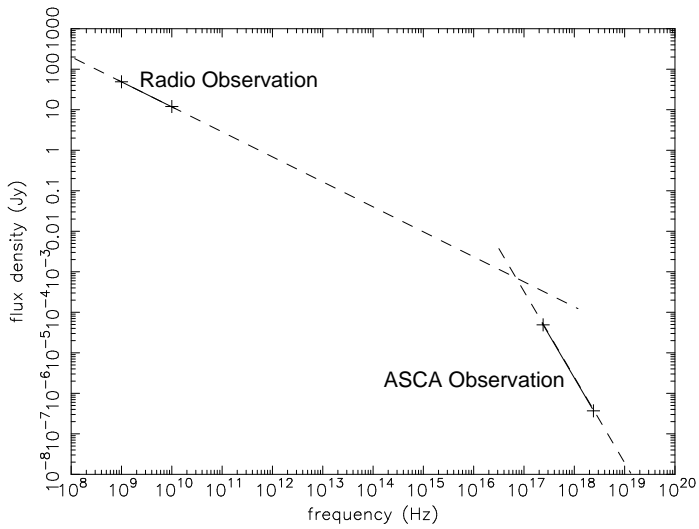


Fig. 4.. The wide band spectrum from radio to X-ray band. The solid lines mean observational flux density, whereas the dashed lines are extrapolated flux.

Table 1. Best-fit parameters for SW shell for a two-temperature plasma and power-law model.\*

Parameters	Component 1	Component 2	Non-thermal component
$kT$ (keV) . . . . .	0.34 (0.30 – 0.38)	23.8 (15.1 – 26.0)	...
$\log nt$ (s cm <sup>-3</sup> ) . . . . .	10.7 (10.6 – 10.8)	10.1 (10.0 – 10.2)	...
O/H <sup>†</sup> . . . . .	3.3 (2.3 – 3.8)	...	...
Ne/H <sup>†</sup> . . . . .	(> 6.7)	...	...
Mg/H <sup>†</sup> . . . . .	(> 4.7)	...	...
Si/H <sup>†</sup> . . . . .	(> 6.5)	...	...
Fe/H <sup>†</sup> . . . . .	2.4 (1.7 – 3.1)	3.3 (2.3 – 6.0)	...
Photon index . . . . .	...	...	3.1 (3.0 – 3.2)
$N_H$ ( $\times 10^{21}$ H cm <sup>-2</sup> ) . . . . .	3.2 (2.9 – 3.8)	3.2 <sup>‡</sup>	3.2 <sup>‡</sup>
Flux (erg cm <sup>-2</sup> s <sup>-1</sup> ) <sup>§</sup> . . . . .	$1.5 \times 10^{-10}$	$6.2 \times 10^{-11}$	$1.0 \times 10^{-10}$

\* Parentheses indicate 90% confidence regions for one relevant parameter.

† Abundance ratio relative to the solar value.

‡ Common with component 1.

§ In the 0.7–10.0 keV band.

Table 2. Normalized flux of each region for the thermal and non-thermal components.\*

Region	thermal component (erg s <sup>-1</sup> cm <sup>-2</sup> arcmin <sup>-2</sup> )		non-thermal component (erg s <sup>-1</sup> cm <sup>-2</sup> arcmin <sup>-2</sup> )	N/T <sup>†</sup>	reduced $\chi^2$
	component 1	component 2			
SW-1 shell . . . . .	$6.9 \times 10^{-13}$	$1.6 \times 10^{-13}$	$8.9 \times 10^{-14}$	0.1	520.5905/291
SW-2 shell . . . . .	$5.1 \times 10^{-13}$	$2.3 \times 10^{-13}$	$4.2 \times 10^{-13}$	0.6	1056.154/673
NE shell . . . . .	$2.5 \times 10^{-14}$	$3.1 \times 10^{-14}$	$1.8 \times 10^{-13}$	3.2	409.3046/256
Inner region . . . . .	$3.2 \times 10^{-16}$	$4.3 \times 10^{-14}$	$5.8 \times 10^{-14}$	1.3	135.1856/85

\* In the 0.7–10.0 keV band.

† Flux ratio of the non-thermal to the thermal (component 1 + component 2).